# CUME EXAM # 405 with Suggested Solutions

This exam is worth 40 points. It is based on the accompanying preprint by Linder and Mordasini (2016), "Evolution and Magnitudes of Candidate Planet Nine" arXiv:1602.07465. A grade of 70% or higher is expected to be a passing grade. You may use a calculator, but only for algebraic and trigonometric types of calculations — you may NOT use a calculator to store formulae, constants, etc.

Things You Might Need to Know

Filter	Central $\lambda$ ( $\mu$ m)
Johnson Filters	
V	0,55
R	0.64
I	0.82
L	3.45
N	10.5
Q	21
WISE Filters	
W1	3.4
W2	4.6
W3	-12
W4	22

#### **Additional Instructions**

- Start each question on a new page and then staple your packet of pages together at the end. Put your name on every page.
- Write legibly! If I cannot read your writing, you likely will not receive as much credit as you deserve because I won't understand what you are trying to convey.

1. Given the orbital semimajor axis value listed in the paper and assuming an orbital eccentricity of e=0.6, compute the perihelion and aphelion distances for Planet X. (2 points)

The orbital semimajor axis was given in the paper to be 700 AU. We can compute  $\mathbf{r}_{peri}$  and  $\mathbf{r}_{ap}$  using

$$r = \frac{a(1 - e^2)}{1 + e\cos\theta} \tag{1}$$

where  $\theta=0^{\circ}$  corresponds to  $r_{peri}$  and  $\theta=180^{\circ}$  corresponds to  $r_{ap}$ . Plugging in the above values yields  $r_{peri}=280$  AU and  $r_{ap}=1120$  AU.

2. The authors state on p. 2 that "the wavelength of maximum blackbody emission at a temperature of 47 K follows from Wien's law and is 62  $\mu$ m..." Based on the information in Figure 1, calculate the range of peak blackbody wavelengths for Planet X from the time of its formation to 8 billion years after its formation. (4 points)

Using Wien's Law,  $\lambda_{max}$  T = 2.898 × 10<sup>-3</sup> m K, we can solve for  $\lambda_{max}$ . We can read off the temperatures of Planet X over the age of the solar system from the lower left panel of Figure 1 (red curve). Plugging in T = 100 K at time t(0) and T = 40 K at time t(8 by), we get  $\lambda_{max}(0) = 29 \ \mu \text{m}$  and  $\lambda_{max}(8 \text{ by}) = 72.5 \ \mu \text{m}$ . So the planet continues to cool off over the age of the solar system, and its peak blackbody wavelength moves to progressively longer wavelengths.

3. Also on p. 2, the authors state that "the equilibrium temperature is slowly rising due to the Sun's evolution." Based on the information shown in the lower left panel of Fig. 1, calculate the change in the Sun's luminosity from the time of its formation to 8 billion years later, assuming that nothing else had changed about Planet X over that same time period. (5 points)

From the lower left panel of Figure 1, we can see that the equilibrium temperature of Planet X increased from 10 K to 12 K over the 8 billion year time period. Assuming that nothing else about Planet X had changed, the change in equilibrium temperature would be due to the increase in the Sun's luminosity over that same time period. We can use the equation for equilibrium temperature to get a ratio of the two solar luminosities: We need to equate the incoming solar flux to the outgoing thermal radiation:

$$F_{in} = \frac{L_{\odot}}{4\pi a^2} (1 - A_b) \pi R^2 \tag{2}$$

and

$$F_{out} = 4\pi R^2 \epsilon \sigma T_{eq}^4 \tag{3}$$

where a is Planet X's orbital semi-major axis, R is its radius,  $A_b$  is the Bond albedo,  $\epsilon$  is its emissivity, and  $T_{eq}$  is the equilibrium temperature. Equating  $F_{in}$  and  $F_{out}$  and solving for  $T_{eq}$ , we get

$$T_{eq} = \left[ \frac{L_{\odot}(1 - A_b)}{16\pi\sigma a^2} \right]^{1/4} \tag{4}$$

Assuming everything else remains the same over the time period in question, then

$$\left(\frac{T_f}{T_i}\right)^4 = \frac{L_{\odot,f}}{L_{\odot,i}} \tag{5}$$

$$\frac{L_{\odot,f}}{L_{\odot,i}} = \left(\frac{12}{10}\right)^4 = 2.07\tag{6}$$

So the Sun's luminosity increased by about a factor of 2 over the 8 billion year time period.

4. Compute the *change* in the luminosity of Planet X (as shown in the upper right panel of Fig. 1) from the time of solar system formation to the present day by using information shown in the left panels of Fig. 1. If you detect any discrepancies between the values you calculate and those shown in the upper right panel Fig. 1, comment on their possible source(s). [Hint: you do not need to compute absolute luminosity numbers to get a sense of how it changed from one time to another.] (5 points)

Luminosity is given by  $L = 4\pi R^2 \sigma T^4$ . We can again use ratios to get a sense of how Planet X's luminosity changed from the time of solar system formation to the present day.

$$\frac{L_{now}}{L_o} = \left(\frac{R_{now}^2 T_{now}^4}{R_o^2 T_o^4}\right) = \left(\frac{3.7}{4.8}\right)^2 \left(\frac{47}{102}\right)^4 = 0.027 \tag{7}$$

According to the upper right panel of Fig. 1,  $\frac{L_{now}}{L_o} = \frac{0.006}{0.3} = 0.020$ . This is pretty close to what we got from our simple ratio. Possible sources of the minor discrepancy could be inadequate treatment of the planet's opacity sources and/or internal composition and interior structure, all of which can influence the flow of heat from the interior to the surface of Planet X.

5. Based on the blackbody curves in the lower right panel of Fig. 1, calculate the expected difference in the apparent magnitudes of Planet X between the Q and V bands. Compare your result to what is shown in the left panel of Fig. 2. (5 points)

We can use the magnitude-flux relationship:  $m_1 - m_2 = -2.5 log \left(\frac{F_1}{F_2}\right)$ . The two bands of interest are Q (21  $\mu$ m) and V (0.55  $\mu$ m), where the intensities of Planet X are  $\sim 10^{-1}$  and  $5 \times 10^{-5}$  Jy, respectively. [The value used for the Q band intensity depends significantly on which time is considered; here I estimated it for  $3 \times 10^9$  years after solar system formation.] Plugging in the above values gives  $m_V - m_Q = 8.25$ . If we compare the magnitudes shown in Figure 2 (left panel), we see that  $m_V$  ranges from 23 to 18 and  $m_Q$  ranges from 12 to 9.5. So the  $\Delta m$  values vary from 11 to 8.5, which is about on par with what we calculated.

6. Based on the right panel of Fig. 2, in which WISE filter(s) and at what time(s) would we have the best chance of detecting Planet X? Explain your answer. You may assume that the time range shown on the x-axis of that graph represents one complete orbit of Planet X. (3 points)

In order to have a reasonable chance of detecting Planet X, we need the magnitude curves to fall below (i.e. to a smaller magnitude value than) the respective S/N=5 limits for the four WISE filters shown by the dashed lines. This only happens for the W1 filter, and even then only when the object is close to perihelion (time  $\sim 16{,}000$  years). This is consistent with the conclusion made by the authors at the end of Section 4.2.

7. Imagine that Planet X is not a planet, but instead a remnant of a much larger object that underwent a major collision, leaving behind great quantities of debris with a typical post-impact size distribution (lots of smaller particles, fewer larger particles). Assuming that the collision happened at the location corresponding to Planet X's perihelion, calculate the maximum size of particle that will remain in orbit around the Sun rather than being blown away by radiation pressure. [Hint: you must balance two forces!] You may assume that the particles are perfectly absorbing. (6 points)

We need to balance the gravitational force due to the Sun and the force of radiation pressure on the particle to determine at which particle size the two balance out. These two expressions are given by the following:

$$F_g = \frac{GM_{\odot}m}{r_o^2} = \frac{L_{\odot}\pi R^2 Q_{pr}}{4\pi r_o^2 c} = F_{rad}$$
 (8)

where  $L_{\odot}$  is the Sun's luminosity, R is the particle radius,  $r_o$  is the particle's distance from the Sun, and  $Q_{pr}$  is a radiation pressure coefficient (and is = 1 for completely absorbing particles). We can rewrite the mass of the particle, m, as  $\rho(\frac{4}{3}\pi R^3)$ . Plugging that into Eq. (8) and solving for R gives  $R \sim 0.2 \ \mu m$  (depending on your choice for  $\rho$ ).

8. The authors state in the last paragraph of the paper that Planet X is expected to have an astrometric motion of  $\sim 0.3$ "/hr. Let's compare that to

something closer to get a sense of how difficult it will be to detect a moving target at the distance of Planet X. Compute the expected angular motion (in arcseconds per hour) for an object located in the asteroid belt – stating all your assumptions – and compare your result to that quoted above for Planet X. (5 points)

The angular motion of something in the asteroid belt can be computed to first order by estimating the angular projection of the object's orbital motion. In other words, we are neglecting the Earth's parallactic motion. In that case, assume an orbital semimajor axis of 3 AU for an object in the asteroid belt and determine the object's orbital speed:

$$v_{orb} = \sqrt{\frac{GM_{\odot}}{r}} \sim 17 \ km/s \tag{9}$$

If we assume that all of the object's motion is tangential to us, then we can use the small angle approximation:

$$sin\theta \approx \theta = \frac{17.2 \ km/s}{3 \ AU \times 1.5 \times 10^8 \ km/AU} = 2.16 \times 10^{-6} \ deg/s = 28 \ arcsec/hr.$$
 (10)

This is MUCH larger than the expected motion of Planet X - no wonder it is going to be so difficult to detect!

9. Give a qualitative explanation for how the rate of gravitational cooling depends on an object's internal composition. Hint: When formulating your response, consider the gravitational potential energy associated with the process of cooling and what its dependencies are. (5 points)

The process of gravitational cooling refers to the release of gravitational potential energy as a planet (or star) contracts. The gravitational potential energy is given as  $U = -\frac{GM(r)dm}{r}$ , where we are considering the object to be made of a series of concentric shells. In that case M(r) is the amount of mass enclosed at some distance r from the center, and dm is the mass of a shell of thickness dr. If we rewrite dm as  $4\pi r^2 \rho dr$  and integrate the expression for U from 0 to R, we get  $U = -\frac{16}{15}G\pi^2\rho^2R^5 = -\frac{3M^2G}{5R}$ . Finally, if we apply the virial theorem and consider that half of this potential energy is radiated away during the collapse, the total energy radiated away is  $U_r = \frac{3M^2G}{10R}$ .

Even if you did not know how to derive this expression, the point is that the gravitational cooling is related to the density<sup>2</sup> and size (or alternatively, to the mass<sup>2</sup>) of the planet. So the internal composition plays an important role in determining the rate of cooling of a contracting planet or star.

### **Evolution and magnitudes of candidate Planet Nine**

Esther F. Linder and Christoph Mordasini

Physikalisches Institut, University of Bern, Sidlerstrasse 5, 3012 Bern, Switzerland

Received 19.02.2016 / Accepted 24.03.2016

#### **ABSTRACT**

Context. The recently renewed interest in a possible additional major body in the outer solar system prompted us to study the thermodynamic evolution of such an object. We assumed that it is a smaller version of Urahus and Neptune.

Aims. We modeled the temporal evolution of the radius, temperature, intrinsic luminosity, and the blackbody spectrum of distant ice giant planets. The aim is also to provide estimates of the magnitudes in different bands to assess whether the object might be detectable

Methods. Simulations of the cooling and contraction were conducted for ice giants with masses of 5, 10, 20, and 50  $M_{\oplus}$  that are located at 280, 700, and 1120 AU from the Sun. The core composition, the fraction of H/He, the efficiency of energy transport, and the initial luminosity were varied. The atmospheric opacity was set to 1, 50, and 100 times solar metallicity.

Results. We find for a nominal  $10~M_{\oplus}$  planet at 700~AU at the current age of the solar system an effective temperature of 47~K, much higher than the equilibrium temperature of about 10~K, a radius of  $3.7~R_{\oplus}$ , and an intrinsic luminosity of  $0.006~L_{\oplus}$ . It has estimated apparent magnitudes of Johnson V, R, I, L, N, Q of 21.7, 21.4, 21.0, 20.1, 19.9, and 10.7, and WISE W1-W4 magnitudes of 20.1, 20.1, 18.6, and 10.2. The Q and W4 band and other observations longward of about  $13~\mu\text{m}$  pick up the intrinsic flux.

Conclusions. If candidate Planet 9 has a significant H/He layer and an efficient energy transport in the interior, then its luminosity is dominated by the intrinsic contribution, making it a self-luminous planet. At a likely position on its orbit near aphelion, we estimate for a mass of 5, 10, 20, and 50  $M_{\oplus}$  a V magnitude from the reflected light of 24.3, 23.7, 23.3, and 22.6 and a Q magnitude from the intrinsic radiation of 14.6, 11.7, 9.2, and 5.8. The latter would probably have been detected by past surveys.

Key words. Planets and satellites: detection - Planets and satellites: physical evolution - Oort Cloud; - Kuiper belt: general

#### 1. Introduction

The presence of another major body in the solar system would be of highest interest for planet formation and evolution theory. Based on the observed peculiar clustering of the orbits of trans-Neptunian objects (Brown et al. 2004; Trujillo & Shoppard 2014) and after analyzing several earlier hypotheses (de la Fuente Marcos & de la Fuente Marcos 2014; Iorio 2014; Madigan & McCourt 2016), Batygin & Brown (2016) have recently proposed that a  $\sim 10~M_{\oplus}$  planet might be present in the outer solar system at a distance of several hundred AU from the Sun. Following the historical example of Neptune, the next step would be the observational discovery of the object. Depending on its specific properties, because of faintness, slow motion on the sky, and confusion with Galactic background stars, the object might in principle have evaded detection up to now. In this article we present predictions for the physical properties of a planet such as the one proposed, which is important to determine whether it might be detectable. Based on the most likely mass and the extrasolar planetary mass-radius relation (e.g., Gettel et al. 2016), we assume that candidate Planet 9 has the same basic structure as Uranus and Neptune. As already speculated by Batygin & Brown (2016), it might be an ejected failed giant planet core. Planets of this type frequently from in planet formation simulations that are based on the core accretion theory (Mordasini et al. 2009) and may be scattered to large distances by giant planets (Bromley & Kenyon 2011).

#### 2. Evolution model

Our planet evolution model (Mordasini et al. 2012) calculates the thermodynamic evolution of planetary parameters (such as luminosity or planetary radius) over time for a wide range of initial conditions. The planet structure is simplified by assuming that the central part consists of iron. This is wrapped in a silicate mantel followed by a possible water ice layer and finally a H/He envelope. To derive the luminosity, the contributions of the contraction and cooling of the gaseous envelope and of the solid core can be included, as well as radiogenic heating. In the default configuration of the model, the interior is assumed to be adiabatic and to fully contribute to the planet luminosity, as is probably the case for Neptune, but not for Uranus (Nettermann et al. 2013). Alternatively, the solid part (core) of the planet can also be assumed to be isothermal or to be at zero temperature. In the latter case, it does not contribute to the gravothermal energy release (Baraffe et al. 2008). The atmospheric model is gray and modeled with the condensate-free opacities of Freedman et al. (2014). Stellar irradiation is included through the Baraffe et al. (2015) tracks. The simulations start at 10 Myr at a prespecified initial luminosity.

#### 3. Simulations

Based on the nominal scenario in Baygin & Brywn (1046), we started our study with a planet of  $10~M_{\oplus}$  at a semimajor axis of 700 AU. Given the typical core-to-envelope mass ratio found in planet formation simulations (Mordavini et al. 2014), we assumed the core and envelope masses to be 8.6 and 1.4  $M_{\oplus}$ , respectively. This is compatible with the estimated H/He mass

fractions of Uranus (12-15%) and Neptune (16-19%, Guillot & Gautier 2014). The initial luminosity was also taken from the formation simulations and set to 1.41  $L_4$ , similar as in Fortney et al. (2011). The core composition is 50% water ice (referred to as "ice" in the following), 33.3% silicates, and 16.7% iron (this mix of silicate and iron is referred to as "rock" in the following). The atmospheric opacity corresponds to an enrichment of 50 times solar. This first simulation is called the "nominal case" in the following. To calculate magnitudes, we used a blackbody spectrum for the planet, the Vega spectrum from Bohlin & Gilliland (2004), and tabulated filter transmissions (Mann & von Braun 2015; Bessell & Brett 1988; Persson et al. 1998; De Buizer & Fisher 2005; Jarrett et al. 2011) . We calculated the reflected flux from the object assuming it is at full phase. In the nominal model, the Bond and geometric albedo were set to 0.31 and 0.41. These are the values for Neptune (Traub & Oppenheimer 2010).

For non-nominal simulations of the  $10~M_{\oplus}$  planet, the initial luminosity was set to a value 10 times higher and lower. Such a variation covers the spread of post-formation luminosities found in our formation simulations (Mordasini et al. 2014). We also increased the H/He fraction to 50% to explore a very efficient gas accretion during formation. The consequences of an isothermal instead of an adiabatic temperature structure in the core were studied as well. The core composition was also varied, assuming a purely rocky and purely icy core. We also varied the opacity of the atmosphere, corresponding to an enrichment of 1 and 100 times solar, which is approximately the enrichment of carbon in Uranus and Neptune (Guillot & Gautier 2014). To account for the high eccentricity of the object, the semimajor axis was changed to 280 and 1120 AU.

We also studied Uranus-like cases where we set the Bond and geometric albedo to 0.30 and 0.51 (Traub & Oppenheimer 2010; Guillot & Gautier 2014). It is well known that the current intrinsic luminosity of Uranus is much lower than predicted by evolutionary models that assume that the interior is fully adiabatic (e.g., Fortney et al. 2011; Nettelmann et al. 2013). As suggested by Podolak et al. (1991), this might be due to a statically stable interior that is unable to convect because of compositional gradients. If the heat is transported by conduction instead of convection, a strongly reduced flux is expected (Nettelmann et al. 2013). A simple way to model this situation is to exclude a central part of the planet interior from contributing to the luminosity. With this approach, Nettelmann et al. (2013) found that the low luminosity of Uranus can be matched if about half of its mass does not contribute. To investigate this possibility, we ran models where the core does not contribute to the planet luminosity, which means that we deprived the planet of its primary reservoir of gravothermal energy. An alternative explanation for the low intrinsic luminosity of Uranus might in principle be that it was already very cool when it formed, although this appears rather unlikely from formation models (Stevenson 1982). To simulate such a situation, we also ran a model where the initial luminosity was chosen such that the present-day luminosity is a factor 10 lower than in the nominal case. This factor 10 approximately corresponds to the ratio of Neptune's intrinsic luminosity and to the upper limit for the intrinsic luminosity of Uranus (Garllot & Gautier 2014).

Finally, the planet mass was varied to 5, 20, and  $50 M_{\oplus}$  with envelope mass fractions of 10, 21, and 37 % as representative for the aforementioned formation simulations, from which we also took the initial luminosities of 0.32, 6.27, and 44.96  $L_{\odot}$ , respectively.

#### 4. Results

#### 4.1. Nominal simulation

Figure 1 shows the evolution of the radius, luminosity, temperature, and blackbody spectrum for the nominal case. The top left panel shows that the 1 bar radius today is at 3.66  $R_{\oplus}$  equal to 23'300 km. The top right panel shows the decrease of the total, envelope, core, and radiogenic luminosity in time. The current total intrinsic luminosity is  $0.006 L_{\perp}$ , with a dominant contribution from the core thermal cooling. For comparison, Neptune has an intrinsic luminosity of 0.01  $L_{4}$  (Guillot & Gautier 2014). The bottom left panel shows that the current temperature at  $\tau=2/3$  is 47 K. The wavelength of the highest black body emission at a temperature of 47 K follows from Wien's law and is 62  $\mu$ m in the far-infrared (far-IR). This temperature is much higher than the equilibrium temperature of about 10 K at 700 AU. The planet energy budget is thus dominated by the intrinsic flux. For this, the assumption of a fully convective interior is critical. Without efficient energy transport, the planet intrinsic luminosity could be much lower, as for Uranus (Nettelmann et al. 2013). Such an Uranus-like situation is considered in Sect. 4.3. The temperature at the 1 bar level is about 66 K, while at the envelope-core boundary around 2100 K are reached. The equilibrium temperature also rises slowly as a result of the solar evolution. The evolution of the blackbody spectra is shown in the bottom right panel. The reflected contribution at wavelengths shorter than  $\sim 13 \mu m$ remains nearly constant, whereas the higher and varying intrinsic contribution in the mid- and far-IR follows the intrinsic luminosity. Non-gray effects can significantly modulate the actual spectrum (e.g., Traub & Oppenheimer 2010).

#### 4.2. Magnitudes in various bands during one orbit

For an age of 4.56 Gyr, when the luminosity is  $0.006 L_{4}$ , we carried out a simulation with nominal parameters, for which we varied the planet heliocentric distance in time, as found from solving the Kepler equation. The thermal timescale of the atmosphere (outer radiative zone) is of about 100 years, as found from dividing the atmospheric thermal energy content by the luminosity. This is much shorter than the orbital timescale, which means that the atmosphere is expected to adapt to the varying stellar irradiation without significant thermal inertia. Figure 2 shows the apparent magnitudes for various bands for the nominal case during one orbit around the Sun at a semimajor axis of 700 AU and an eccentricity of 0.6, as proposed by Batygin & Brown (2016). At a distance of 700 AU, the planet has estimated apparent magnitudes of Johnson V, R, I, L, N, Q of 21.7, 21.4, 21.0, 20.1, 19.9, and 10.7. In the Q filter the intrinsic luminosity of the planet is visible. The planet is thus much brighter in the mid- and far-IR than in the visual or near-IR. The Wide-Field Infrared Survey Explorer (WISE) magnitudes W1, W2, W3, and W4 are shown in the right panel; they are 20.1, 20.1, 18.6, and 10.2 at 700 AU. The magnitudes at other heliocentric distances rare simply found from the  $1/r^4$  dependency for the reflected flux, meaning that at perihelion it is 4 mag brighter and 2 mag dimmer at aphelion, while for the intrinsic flux (Q and W4), the  $1/r^2$ dependency means that at perihelion it is 2 mag brighter and 1 mag dimmer at aphelion. The W3 band picks up both reflected and intrinsic radiation. In the right panel the WISE S/N=5 limits of W1=16.8, W2=15.6, W3=11.3, and W4=8.0 (Lebana 2004) are also shown, indicating that it is only possible to see the object with WISE close to perihelion with the W1 filter. The actual de-

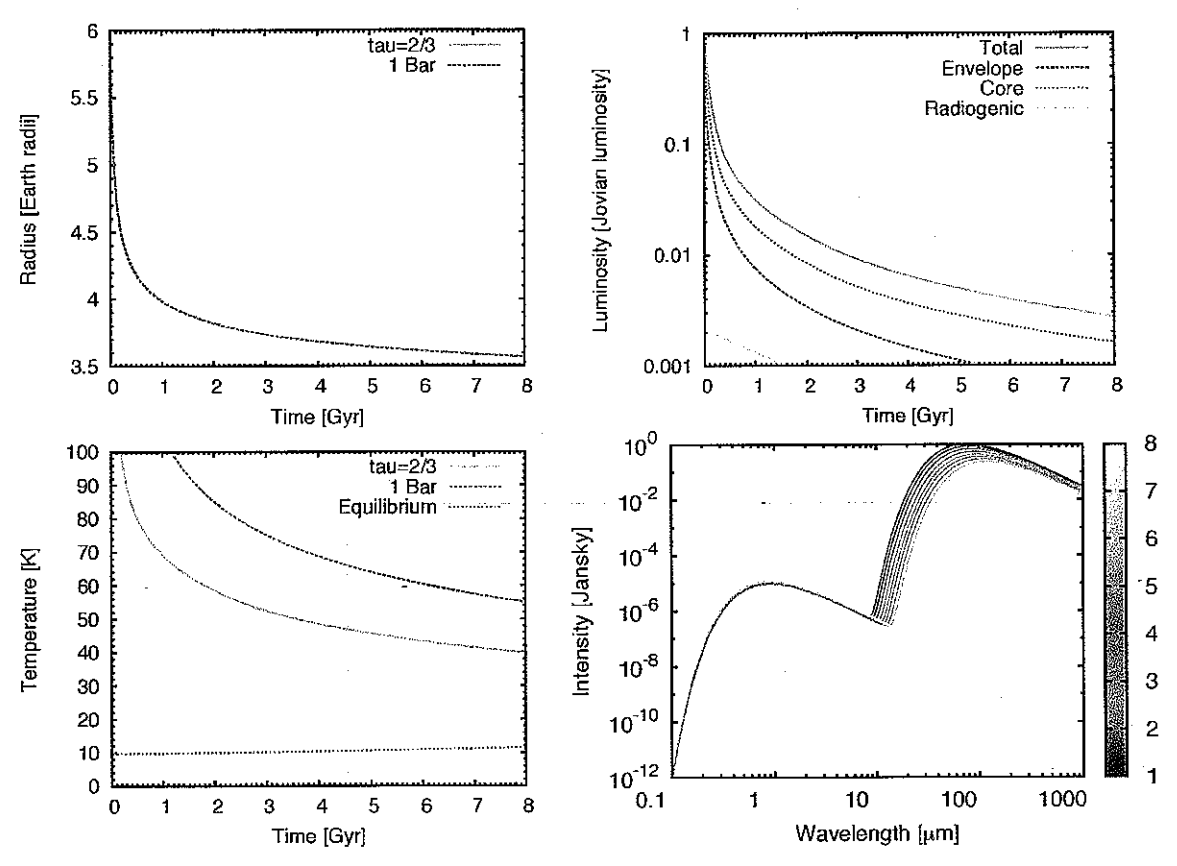


Fig. 1: Temporal evolution of fundamental properties of a 10  $M_{\oplus}$  planet at 700 AU with a 1.4  $M_{\oplus}$  H/He envelope, a core consisting of 50% ice and 50% rock, and an atmospheric opacity of 50 times solar. Top left: Radius. Top right: Intrinsic luminosity. Bottom left: Temperature. Bottom right panel: Blackbody spectrum where the age in gigayears is given by the color code.

tection limit of the survey of Lubman (2014) is W2=14.5, given by the ability of detecting an object in multiple epochs.

## 4.3. Long-term evolution of the magnitudes and non-nominal simulations

To understand the effect of the assumptions made for the nominal model, we simulated evolutionary tracks using different initial conditions and model settings. In the first group of simulations the planets all have a total mass of  $10~M_{\oplus}$ , while in the second set of simulations we considered masses of 5, 20, and 50  $M_{\oplus}$ .

Effect of different initial conditions. In the top left panel of Fig. 3 we show the change in luminosity over time for different initial luminosities and also for a nominal planet but with a semi-major axis of 5 AU. This latter simulation was made to study the scenario in which the planet first evolves closer to the Sun before it is ejected to its current position. It is evident that neither the change in starting luminosity (at least for a variation by two orders of magnitude, as indicated by the formation model) nor the change in semimajor axis has a significant effect on the luminosity of the planet today. From the current thermodynamic properties of the planet it is therefore difficult to constrain the moment in time when the planet underwent a possible scattering

outward from its potential formation region near the other giant planets.

Effect of different internal structures. The top right panel in Fig. 3 shows the temporal change in apparent Q and V magnitude for different internal structures; for a planet that has an envelope mass fraction of 50% instead of 14%, and for a planet whose core is isothermal instead of adiabatic. In the former case, the intrinsic luminosity increases slightly. At the same time, the magnitude in the Q band increases from 10.7 to 12.0 mag, meaning that the planet becomes dimmer in this band. This is a result of the decrease of the planet effective temperature because the increase in planet radius that is due to the higher H/He mass fraction overcompensates for the higher luminosity. For an isothermal core, the planet heat reservoir in the core is reduced compared to the adiabatic case because the core is entirely at the temperature of the envelope-core boundary. This results in a luminosity that is lower by about 15% than in the nominal case. This is a much weaker change than occurs if the core contribution is entirely neglected, as we show below. We therefore recover the finding of Baraffe et al. (2008), who reported that the nature of the heat transport in the core is not as important as is including the core thermal contribution as such. In the V band, where the magnitudes range from 21.0 to 21.8, the case with a 50% envelope mass fraction is the brightest because of its significantly larger radius of 5.22  $R_{\oplus}$ , whereas the magnitudes of the

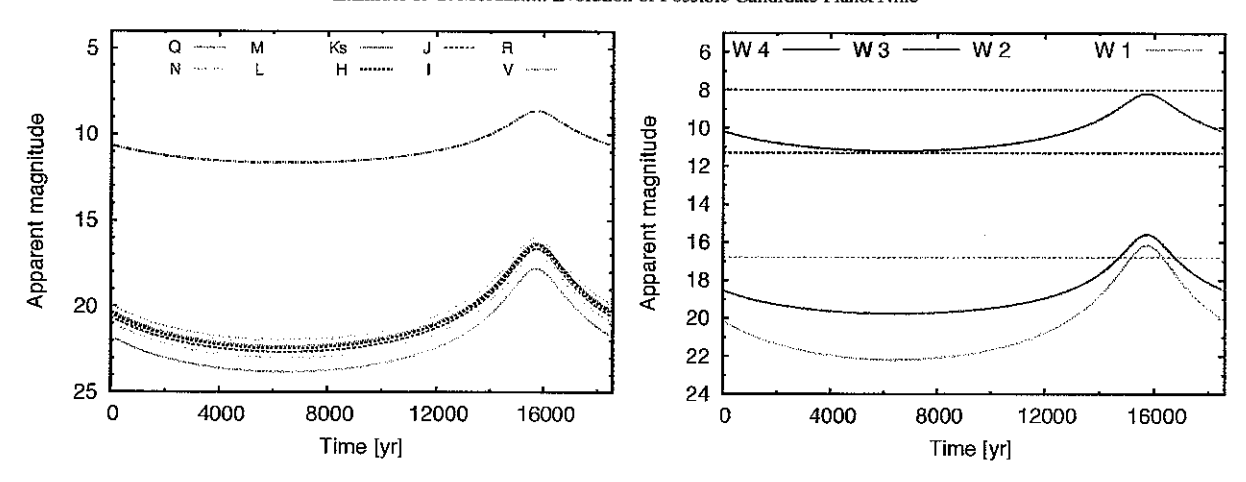


Fig. 2: Present-day apparent magnitudes for the nominal  $10 M_{\oplus}$  planet during one orbit around the Sun at a=700 AU and e=0.6. Left panel: Johnson V to Q. Right panel: WISE filters, together with S/N=5 limits shown by dashed horizontal lines (Luhman 2014).

nominal and isothermal case overlap because they nearly have the same radius.

Core composition. The influence of a change in core composition on the magnitudes compared to the nominal case is weak. For the V band, the planet with a rocky core is the faintest (21.9 mag), while the planet with a purely icy core is the brightest (21.6 mag), owing to a radius that is  $0.3 R_{\oplus}$  smaller and larger than in the nominal case. In the Q band the planet with the purely icy core is also brighter (10.2 mag) than for a purely rocky core (11.5 mag), now because of the higher heat capacity of water (Barafie et al. 2008).

Atmospheric opacity. A variation of the opacities corresponding to an enrichment of 1, 50, and 100 solar has a very weak effect on the V- and Q-band magnitudes for the  $10~M_{\oplus}$  planet (differences smaller than 0.3 mag).

Orbital distance. We simulated the evolution of the 10  $M_{\oplus}$  planet at a fixed distance of 280 and 1120 AU (the estimated perihelion and aphelion distances of candidate Planet 9) instead of 700 AU. The resulting present-day physical properties of the planet are virtually unchanged, showing that the interior evolution proceeds as if the planet were in isolation, as already observed for the evolution at 5 AU. This means that the change of the planet magnitude during its orbit is simply due to the change in its heliocentric distance. For example, the V- and Q-band magnitudes at aphelion are then 2.04 and 1.02 mag fainter than at 700 AU.

Uranus-like cases. In the bottom left panel of Fig. 5 two simulations of 10  $M_{\oplus}$  planets with albedos like that of Uranus are shown together with the nominal case. One simulation was conducted without core contribution to the gravothermal heat release, which mimics stabilizing compositional gradients ("no core cooling"). This planet has a present-day luminosity of 0.0013  $L_4$ , about a quarter of the nominal case,  $R=3.48 R_{\oplus}$ , and  $T_{\rm eff}$ =33 K. In the second simulation the starting luminosity was chosen such that the planet has a present-day luminosity that is a tenth of the luminosity in the nominal case ("low L today"), mimicking a very "cold" formation. The planet has a present-day radius of  $3.42 R_{\oplus}$  and an effective temperature of 27 K. The consequences for the V-band magnitude for these two cases are limited, with a variation of only 0.3 mag. Since the V band detects the reflected flux, the difference in magnitude can be explained by the small difference in radius between these cases of  $0.2R_{\oplus}$ .

In contrast, the effect on the Q magnitude is much stronger, as expected. Instead of 10.7 mag as in the nominal case, Q is 16.4 for the "no core cooling" and 19.6 for the "low L today" case. The efficiency of heat transport in candidate Planet 9 therefore strongly influences its brightness in the IR or at mm-wavelengths (Cowan et al. 2016), meaning that observations in this regime might be able to constrain whether candidate Planet 9 has an internal structure like Neptune or rather like Uranus (Cowan et al. 2016). The different temporal evolution of the Q magnitude for the "low L today" case is also quite clear. This can be explained by the fact that the starting luminosity is already so low that the planet barely evolves at all, and even the Q band now mirrors mostly the evolution of the Sun.

Candidate Planet 9 as a super-Earth. As a last non-nominal model with M=10  $M_{\oplus}$ , we also examined the possibility that candidate Planet 9 might be a super-Earth without any significant atmosphere and an Earth-like interior. We found that the planet would have a radius of about 1.9  $R_{\oplus}$ . Assuming that the silicate mantel has a chondritic abundance of radionuclides (Mordavini et al. 2012), we found that its radiogenic luminosity is at the current age of the solar system about  $6.8 \times 10^{-4} L_{\perp}$ , which is remarkably only eight times lower than the total luminosity in the nominal case and about five times higher than the Earth's intrinsic luminosity (Kamland Collaboration et al. 2011). For the Earth it is estimated that about half of the intrinsic luminosity is radiogenic, and the other half originates from delayed secular cooling. The effective temperature is 38 K, only 9 K lower than in the nominal case because of the smaller radius, and the apparent magnitudes in V and Q are 23.2 and 15.2.

Effect of the mass. In the bottom right panel of Fig. 3 we show apparent magnitudes in the V and Q band for the nominal planet and planets where the mass relative to the nominal case was varied. In general, the objects are brighter in the Q than in the V band. Since in the V band the reflected light of the Sun is visible, the objects become slightly brighter with time, corresponding to the evolution of the Sun. By contrast, the Q band shows the intrinsic radiation of the planet, and the planets slowly become fainter as a result of cooling. In addition to the nominal  $10~M_{\oplus}$  case, the apparent magnitude evolution is shown in the figure for planets of 5, 20, and  $50~M_{\oplus}$ . These planets have a present-day radius of 2.92, 4.62, and  $6.32~R_{\oplus}$ , an intrinsic luminosity of 0.0018, 0.016, and 0.078  $L_{+}$ , and an effective temper-

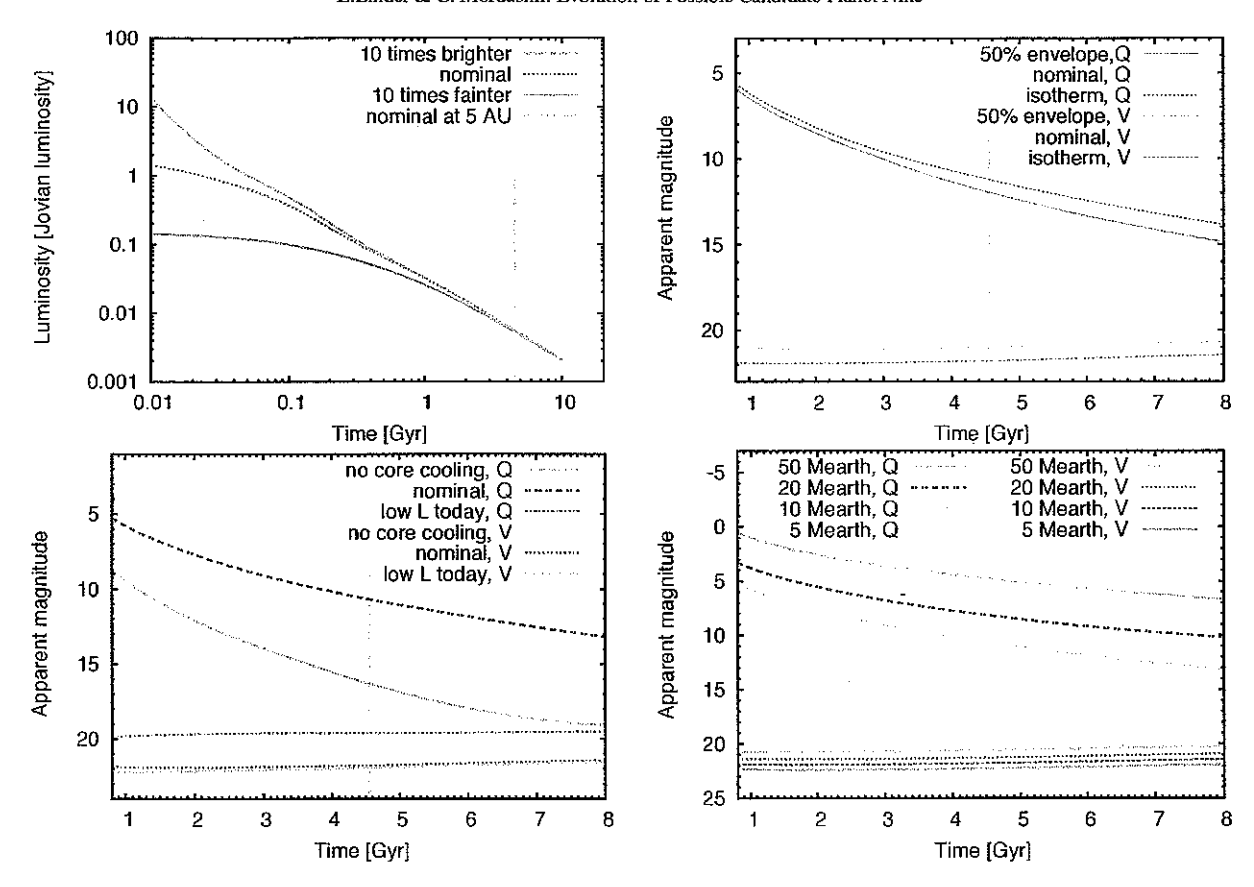


Fig. 3: Top left: Intrinsic luminosity over time for different initial conditions. Top right: Apparent magnitudes over time for different internal structures. Bottom left: Apparent magnitudes for Uranus-like cases. All these three panels are for a 10  $M_{\oplus}$  planet. Bottom right: Evolution of the apparent magnitudes in V and Q for the nominal case (10  $M_{\oplus}$ ) and planets with masses of 5, 20, and 50  $M_{\oplus}$ . All apparent magnitudes are for a distance from the Sun of 700 AU.

ature of 40, 54, and 69 K, respectively. The V-band magnitudes are 22.3, 21.3, and 20.6 mag, and the Q-band magnitudes are 14.6, 8.2, and 5.8 mag, respectively.

#### 5. Discussion and conclusion

Motivated by the recent suggestion by Batygin & Brown (2016) that there might be a possible additional planet in the solar system, the evolution in radius, luminosity, temperature, and blackbody spectrum of a 10  $M_{\oplus}$  planet at 700 AU was studied. We assumed it to be a smaller version of Uranus and Neptune. For an adiabatic interior, we found that the radius of such an object today would be about 3.66  $R_{\oplus}$ . The present intrinsic luminosity of the planet would be about  $0.006 L_{+}$  with the highest contribution coming from the thermal cooling of the core. The effective temperature of the object would be much higher with 47 K than its equilibrium temperature of 10 K, meaning that the planet emission would be dominated by its internal cooling and contraction. Its intrinsic power would be about 1000 times higher than its absorbed power, making it a self-luminous planet. For comparison, Jupiter's intrinsic power is about half as high as its absorbed power (Garllot & Gardier 2014). This dominance would also be visible in the evolution of the blackbody spectrum of the planet, where the evolving intrinsic flux would be much higher than the reflected flux. This also means that the planet would be much brighter in the mid- and far-IR than in the visual and near-IR.

The effect on the apparent magnitude of the planet in the V and Q band was studied for different initial conditions, internal structures, different model assumptions regarding the efficiency of heat transport in the interior, and for a variation in the planet core composition, atmospheric opacity, semimajor axis, and mass. For an adiabatic interior (possibly as in Neptune, Nettelmann et al. 2013), the strongest influence on the Q band comes from the planetary mass, whereas the strongest influence on the V band comes from the planet semimajor axis. This is expected because in the Q band, the intrinsic luminosity of the planet is visible, which is most sensitive to its mass. In contrast, the reflected light is detected in the V band, which is most sensitive to the planet distance from the Sun. For an inefficient heat transport in the interior, possibly as in Uranus, we found that the object could be much dimmer in the Q band by 6 to 9 magnitudes, making it much harder to detect at long wavelengths. The V magnitude, in contrast, is only very mildly increased by about 0.3 mag. This means that the ratio of the brightness in the visual and in the mid- and far-IR constrains the nature of the object.

We found that the evolution of the planet interior is almost identical for a semimajor axis of 5 to 1120 AU, meaning that the moment when the planet arrived at its distant position from the Sun is difficult to constrain from the current intrinsic luminosity. An early ejection during the nebular phase at ages of less than 10 Myr could be preferable from a dynamics point of view because the gaseous nebula could then enable the retention of the object on a far bound orbit (Batygin & Brown 2016). On the other hand, for such an early ejection, the planet might be lost due to stellar encounters in the solar birth cluster (Li & Adams 2016). Insights into the planet origin and formation history might be obtained from its chemical composition or spectrum.

Many surveys in various wavelength domains and with different sensitivities were performed in the past. For example, Trujillo & Brown (2003) observed 12% of the sky near the invariable plane in the R band with a sensitivity limit of 20.7 mag. Candidate Planet 9 is most of the time fainter than 22 mag in the R band (Fig. 2), however, and additionally, it is assumed to have an inclination of  $i = 30^{\circ}$  (Batygin & Brown 2016). This means that Trujillo & Brown (2003) had only a very slight possibility of detecting candidate Planet 9. Another study was done by Elliot et al. (2005), who observed the sky within 6° of the ecliptic with a VR filter down to a limit of 22.5 mag. In this survey, the probability of detecting candidate Planet 9 was also low because the planet orbit and the surveyed fields overlapped only slightly. The same is the case for a study by Larsen et al. (2007), who observed the sky in the V filter down to a magnitude of 21 within 10° of the ecliptic. For comparison, at aphelion at 1120 AU, we found V magnitudes of 24.3, 23.7, 23.3, and 22.6 for masses of 5, 10, 20, and 50  $M_{\oplus}$  for candidate Planet 9. Schwamb et al. (2010) studied the sky within 30° of the ecliptic, excluding fields lower than 15° from the Galactic plane. They had a relatively good coverage of the orbit of candidate Planet 9, except when it was near 13 h RA or in front of the Milky Way, which corresponds to the most likely aphelion position of candidate Planet 9 (Brown & Batygin 2016). The survey was made in the R band down to a luminosity of 21.3 mag, whereas we found R magnitudes exceeding 22 mag near aphelion even for a 50  $M_{\oplus}$  version of Planet 9. Sheppard et al. (2011) surveyed the southern sky and Galactic plane down to -25° in the R filter down to a depth of 21.6 mag. The observed fields show a relatively good coverage of the orbit of candidate Planet 9 and also came closest to the requested brightness, but still did not reach it. Additionally, their astrometric precision reaches 0.5"/hr, whereas candidate Planet 9 instead has a movement of around 0.3"/hr (Brown & Batygin 2016). A search in the IR domain was performed by Luhman (2014), who inspected the WISE data for a distant companion to the Sun (see also Schneider et al. 2016). The WISE satellite mapped the whole sky twice and started mapping it a third time. The detection limits of WISE together with our calculated apparent magnitudes for the nominal case were shown in Fig. 2. The possibility for WISE to detect a 10  $M_{\oplus}$  Planet 9 is small because of the brightness limits. However, if the planet were more massive, a detection becomes more probable, at least from the brightness limit alone. Especially a 50  $M_{\oplus}$  mass planet would have been visible in W4 during its entire orbit, which sets an interesting upper mass limit for the planet. In summary, the current null result seems compatible with the properties of the nominal candidate Planet 9, especially if it is at aphelion. In contrast, future telescopes such as the Large Synoptic Survey Telescope with a sensitivity down to R=26 mag (Luhanas 2014) or dedicated surveys should be able to find or rule out candidate Planet This is an exciting perspective.

Acknowledgements. We thank M. R. Meyer, Y. Alibert, K. Heng, S. Udry, K. Zihlmann, and W. Benz for valuable inputs to the discussion. We thank the referee Ravit Helled for a constructive review. E.F.L. and C.M. acknowledge the support from the Swiss National Science Foundation under grant

BSSGI0\_155816 ,,PlanetsIn'Time". Parts of this work have been carried out within the frame of the National Center for Competence in Research PlanetS supported by the SNSF.

#### References

Baraffe, I., Chabrier, G., & Barman, T. S. 2008, A&A, 482, 315 Baraffe, I., Homeier, D., Allard, F., & Chabrier, G. 2015, A&A, 577, A42 Batygin, K. & Brown, M. E. 2016, AJ, 151, 22 Bessell, M. S. & Brett, J. M. 1988, PASP, 100, 1134 Bohlin, R. C. & Gilliland, R. L. 2004, AJ, 127, 3508 Bromley, B. C. & Kenyon, S. J. 2011, ApJ, 731, 101 Brown, M. E. & Batygin, K. 2016, http://www.findplanetnine.com Brown, M. E., Trujillo, C., & Rabinowitz, D. 2004, ApJ, 617, 645 Cowan, N. B., Holder, G., & Kaib, N. A. 2016, ArXiv e-prints, 1602.05963 De Buizer, J. & Fisher, R. 2005, in High Resolution Infrared Spectroscopy in Astronomy, ed. H. U. Käufl, R. Siebenmorgen, & A. Moorwood, 84-87 de la Fuente Marcos, C. & de la Fuente Marcos, R. 2014, MNRAS, 443, L59 Elliot, J. L., Kern, S. D., Clancy, K. B., et al. 2005, AJ, 129, 1117 Fortney, J. J., Ikoma, M., Nettelmann, N., Guillot, T., & Marley, M. S. 2011, Freedman, R. S., Lustig-Yaeger, J., Fortney, J. J., et al. 2014, ApJS, 214, 25 Gettel, S., Charbonneau, D., Dressing, C. D., et al. 2016, ApJ, 816, 95 Guillot, T. & Gautier, D. 2014, Treatise on Geophysics 2nd Edition (Eds. T. Spohn, G. Schubert) Iorio, L. 2014, MNRAS, 444, L78 Jarrett, T. H., Cohen, M., Masci, F., et al. 2011, ApJ, 735, 112 Kamland Collaboration, Gando, A., Gando, Y., et al. 2011, Nature Geoscience, Larsen, J. A., Roe, E. S., Albert, C. E., et al. 2007, AJ, 133, 1247 Li, G. & Adams, F. C. 2016, ArXiv e-prints, 1602.08496 Luhman, K. L. 2014, ApJ, 781, 4 Madigan, A.-M. & McCourt, M. 2016, MNRAS, 457, L89 Mann, A. W. & von Braun, K. 2015, PASP, 127, 102 Mordasini, C., Alibert, Y., & Benz, W. 2009, A&A, 501, 1139 Mordasini, C., Alibert, Y., Georgy, C., et al. 2012, A&A, 547, 112 Mordasini, C., Alibert, Y., Klahr, H., & Henning, T. 2012, A&A, 547, A111 Mordasini, C., Klahr, H., Alibert, Y., Miller, N., & Henning, T. 2014, A&A, 566, A141 Nettelmann, N., Helled, R., Fortney, J. J., & Redmer, R. 2013, Planet, Space Sci., Persson, S. E., Murphy, D. C., Krzeminski, W., Roth, M., & Rieke, M. J. 1998, AJ, 116, 2475 Podolak, M., Hubbard, W. B., & Stevenson, D. J. 1991, Model of Uranus' interior and magnetic field, ed. J. T. Bergstralh, E. D. Miner, & M. S. Matthews (Tucson, AZ: University of Arizona Press), 29-61 Schneider, A. C., Greco, J., Cushing, M. C., et al. 2016, ApJ, 817, 112 Schwamb, M. E., Brown, M. E., Rabinowitz, D. L., & Ragozzine, D. 2010, ApJ, 720, 1691 Sheppard, S. S., Udalski, A., Trujillo, C., et al. 2011, AJ, 142, 98 Stevenson, D. J. 1982, Annual Review of Earth and Planetary Sciences, 10, 257 Traub, W. A. & Oppenheimer, B. R. 2010, Direct Imaging of Exoplanets, ed. S. Seager (Tucson, AZ: University of Arizona Press), 111-156 Trujillo, C. A. & Brown, M. E. 2003, Earth Moon and Planets, 92, 99 Trujillo, C. A. & Sheppard, S. S. 2014, Nature, 507, 471